

SENSITIVITY OF AN ASYMMETRIC, THREE-DIMENSIONAL DIFFUSER TO INLET CONDITION PERTURBATIONS

Emily L. Sayles

Department of Aeronautics and Astronautics
Stanford University
488 Escondido Mall, Building 500 Room 501W, Stanford, CA 94305 USA
esayles@stanford.edu

Christopher J. Elkins

Department of Mechanical Engineering
Stanford University
488 Escondido Mall, Building 500 Room 500K, Stanford, CA 94305 USA
celkins@stanford.edu

John K. Eaton

Department of Mechanical Engineering
Stanford University
488 Escondido Mall, Building 500 Room 501F, Stanford, CA 94305 USA
eatonj@stanford.edu

ABSTRACT

The sensitivity of a three-dimensional asymmetric diffuser to inlet condition perturbations was investigated using dielectric barrier discharge plasma actuators. Previous experimental and computational studies revealed the sensitivity of the separated flow in this diffuser to secondary flows in the inlet duct of the diffuser. By purposefully altering these secondary flows with highly tunable plasma actuators, the diffuser's pressure recovery could be both significantly improved and degraded. Two cases, one with pulsed forcing and another with continuous forcing, were selected for further study using 2D particle image velocimetry (PIV). PIV data were acquired in two streamwise-wall-normal planes. These measurements reveal that the relatively weak spanwise forcing introduced by the plasma actuators changes the size and orientation of the separation bubble. The pulsed forcing case delays separation and results in an improvement in the diffuser's performance while large fluctuations and a larger separation bubble with higher reversed flow velocities in the continuous forcing case contribute to losses in the diffuser's pressure recovery.

INTRODUCTION

Diffusers are ubiquitous in engineering applications. Usually simple in design, they serve to increase the static pressure of a flow by reducing its velocity, albeit often with significant losses. The diffuser that is the subject of the present study was first examined experimentally by Cherry et al (2008). It has a simple design as illustrated in Figure 1, but it develops complex 3D flow features. Magnetic resonance velocimetry (MRV) was used to obtain a

high resolution, three-dimensional, three-component mean velocity database. A stable separation bubble forms early in the expanding section of the diffuser and spreads across one of the two expanding walls of the diffuser. The flow eventually reattaches in a straight exhaust duct where further pressure recovery occurs. A comprehensive direct numerical simulation database (Ohlsson, 2010) corroborates the MRV experiments and provides more detailed information about the turbulence properties. Because of its simple three-dimensional geometry and the existence of a high quality velocity dataset, this diffuser has become a popular test case for validating numerical simulations. Several computational studies have demonstrated the importance of correctly representing the secondary flows in the inlet duct. This sensitivity to inlet conditions suggested that the diffuser's performance could be significantly altered by purposefully perturbing the secondary flows in the inlet duct.

Grundmann et al (2011) took advantage of this sensitivity by placing highly tunable dielectric barrier discharge plasma actuators on one wall of the diffuser's rectangular inlet duct. A wide range of perturbations was generated by varying the actuators' geometry, orientation and operating parameters. Configurations that produced spanwise forcing significantly altered the diffuser's pressure recovery. The actuators were operated in both continuous and pulsed modes with a wide range of duty cycle and modulation frequency combinations. Depending on the orientation, the walljets generated by the actuators could be directed either inwards, towards the centerline of the channel, or outwards, towards the corners. Improvements and degradations of 20% over the baseline case were observed.

Detailed MRV measurements of these cases could not

be replicated because the plasma actuators operate in air and the MRV experiments use water as the working fluid. However, because two of the cases of interest used continuous forcing, the effects on the diffuser's pressure recovery were replicated by placing small delta wing vortex generators in the inlet duct. MRV data reveal marked differences between the two vortex generator cases and the baseline case. Improved pressure recovery was associated with a smaller separation bubble and more uniform velocities at the outlet of the diffuser. The case which decreased the diffuser's performance showed a rapid growth of the separation bubble and the persistence of a high speed core throughout the length of the diffuser which was accompanied by significant in-plane velocities at the diffuser's outlet plane.

Kolade (2010) built a 4x scaled-up version of the Cherry diffuser to acquire 2D PIV measurements augmenting the original MRV data. The goal of the present study is to use PIV measurements in the larger air-flow facility to understand how plasma actuators produce such large changes in diffuser performance.

EXPERIMENTAL SETUP

The experiments were conducted in the Stanford High Reynolds Number Wind Tunnel with a 4:1 scaled-up model of the original test apparatus. The diffuser is fed by a fully-developed rectangular inlet duct with an aspect ratio of 3.33 and a Reynolds number of 26,000 based on a 40mm channel height and a bulk velocity of 10m/s. The diffuser has an area ratio of 4.8 as it expands from the rectangular inlet measuring 133mm by 40mm to a 160mm by 160mm square outlet. The expansion takes place over a length of 600mm, corresponding to 15 channel heights. There are two expanding walls, a more aggressively expanding bottom wall with an angle of 11.3° and a gradually expanding side wall which has an angle of 2.6°. These two expanding walls share an edge and the remaining two walls are flat. A straight-walled square cross-section exhaust duct is attached to the outlet of the diffuser. A series of static pressure taps placed in a line along the inlet channel's centerline are located on the inlet duct, the bottom wall of the diffuser, and the outlet duct.

The dielectric barrier discharge plasma actuators are constructed with 0.08 – mm-thick copper tape electrodes separated by a 1.6mm-thick Macor®ceramic dielectric sheet. The actuators are installed flush with the floor of the inlet channel. A Minipuls 2 High Voltage Generator from GBS Elektronik applies 12kV_{pp} between the high voltage electrodes and the grounded electrodes at frequencies between 5 and 6kHz. Pulsed forcing is obtained by modulating the signal at the desired frequency with the desired duty cycle. The pulsed forcing case for this study has a duty cycle of 40% and a modulation frequency of 5.8Hz. Four 150 – mm-long actuators were placed just upstream of the diffuser's inlet on the floor of the inlet duct. The actuators are oriented in a cascaded configuration with two actuators on either side of the inlet channel's centerline. The spanwise forcing is directed outwards, towards the corners of the inlet channel. An extensive parameter study, described briefly in the results section, led to the selection of the actuators' geometry and operating conditions.

The PIV system consists of a New Wave Solo PIV Nd:YAG laser, a TSI model 610034 Laser Pulse Synchronizer and a TSI model 630047 PIV 13-8 camera with a 1024 x 1280 pixel array and a Nikon Nikkor 50mm lens. The field of view is approximately 72mm by 60mm, yield-

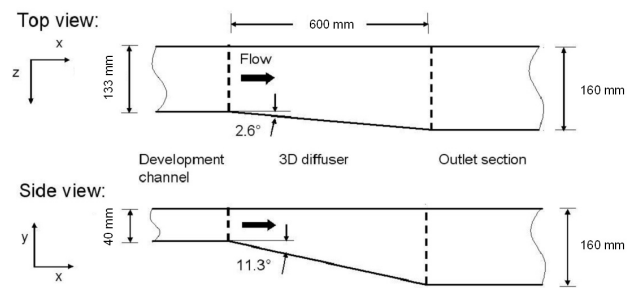


Figure 1. Top and side views of the diffuser.

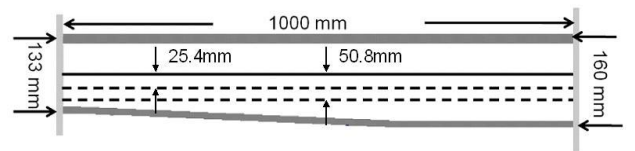


Figure 2. Top view of the diffuser showing the inlet channel centerline and the locations of the two PIV measurement planes. Both measurement planes are offset from the centerline towards the side expanding wall.

ing a resolution of 59μm per pixel and a vector spacing of about 1mm. 5000 image pairs are obtained for each PIV tile and the flow is seeded with 1.5μm polystyrene particles. Processing of the image pairs was performed using a cross-correlation PIV algorithm written at Stanford University (Han 2001) with a minimum correlation coefficient of 0.6 and a 3σ filter which removed pixel displacements that differed by more than 3 standard deviations from the mean pixel displacement. Time delays between frames were selected based on maintaining reasonable maximum pixel displacements within each interrogation region. Flow visualization was used to locate two planes of interest, which are shown in Figure 2. These planes extend in the streamwise and wall-normal directions; both planes are parallel to the non-expanding side wall. Both measurement planes are also offset from the inlet channel's centerline in the direction of the expanding side wall. MRV data show that the separation bubble in the baseline case originates in the corner between the two expanding walls at the very beginning of the diffuser's expansion and spreads completely across the bottom wall of the diffuser by the halfway point, which corresponds to a streamwise location of $x/h = 7.5$. The measurements to date focus on the early development of the separation bubble along the bottom expanding wall of the diffuser.

RESULTS AND DISCUSSION

Plasma Actuator Scaling

An extensive parameter study was conducted in order to properly scale the plasma actuators to obtain the same pressure recovery effects in the scaled-up diffuser model that were observed in the original test apparatus. Notable changes from the original plasma actuators include the use of Macor® instead of layers of kapton tape as the dielectric material, and the four-actuator cascaded configuration instead of a simpler, two-actuator layout. The effectiveness of the actuators for all modes of operation was maximized

at the highest operating voltage, $12kV_{pp}$. Initial scaling of the modulation frequency for pulsed forcing was attempted using a Strouhal number calculated from the bulk velocity, channel height and modulation frequency of the original experiments. The resulting frequency served as a starting point in the search for a modulation frequency which would similarly modify the pressure recovery in the larger diffuser model. A frequency of $5.8Hz$, slightly lower than the $8Hz$ calculated by matching Strouhal numbers, was chosen based on static pressure measurements. Varying the actuators' duty cycle revealed a non-monotonic change in pressure recovery with increasing duty cycle. Continuous forcing produced the worst pressure recovery and a duty cycle of 40% yielded the greatest improvement in performance over the baseline case. The same trends were observed by Grundmann et al (2011). All of the plasma actuator parameter studies were conducted with actuators installed on the floor of the inlet channel, oriented to produce spanwise forcing, directed outwards towards the corners of the inlet duct.

Pressure Recovery

The pressure recovery for the baseline case and the two plasma actuator cases which were chosen for detailed study using PIV are shown in Figure 3. In the baseline case, a rapid initial pressure recovery flattens out due to the growth of the separation bubble along the diffuser's bottom expanding wall. There is further pressure recovery in the constant area exhaust duct as the flow reattaches. The pulsed forcing case also shows a rapid initial recovery of pressure. The pressure distribution shows evidence of a separation bubble farther downstream than the baseline case. The flow is decelerated more smoothly with fewer losses as the pres-

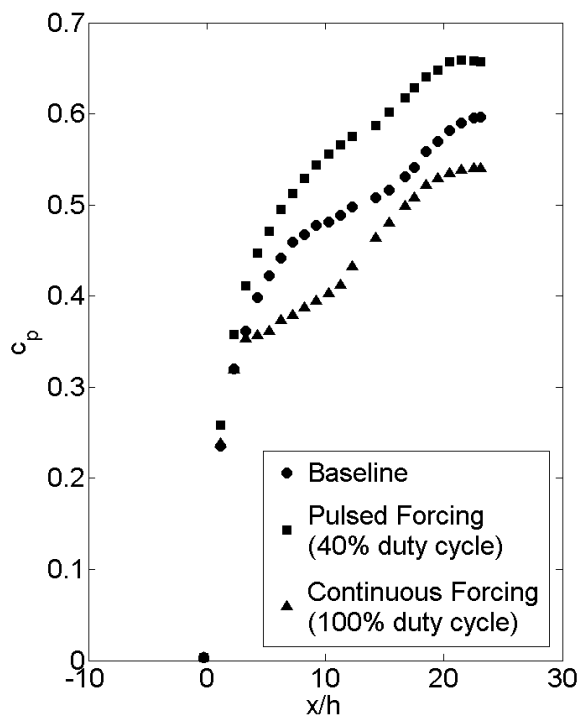


Figure 3. Pressure recovery for the baseline diffuser and the two plasma actuator cases.

sure coefficients reach much higher values at the exit of the diffuser when compared to the baseline case. At the exit of the diffuser, the pressure coefficient is 16% higher than the baseline case. When the actuators are operated continuously there is a dramatic flattening of the pressure recovery very early on in the diffuser's expansion. Although there is reattachment, the flow does not recover to the baseline level due to these early losses. This leads to a 9% decrease in pressure recovery at the outlet of the diffuser.

PIV Measurements

2D particle image velocimetry data were acquired for the baseline case and the two plasma actuator cases in both measurement planes. Several tiles of data along the bottom wall are stitched together to create the mean velocity vector plots shown below.

Figures 5 through 7 display mean velocity vectors at selected streamwise locations in the $25.4mm$ plane. The dashed rectangle in Figure 4 outlines the region in which data were acquired. Figure 4 also shows profiles of streamwise velocity in the midplane of the diffuser obtained by Kolade (2010). The dashed line along the bottom wall demarcates the separation bubble in this plane. For the vector plots, every other vector has been plotted in the wall-normal direction. The full resolution of the PIV data is $1mm$. The velocities are non-dimensionalized by the inlet bulk velocity, $U_{bulk} = 10m/s$.

The profiles in the baseline case, shown in Figure 5, are clearly influenced by the diffuser's adverse pressure gradient. Moving downstream, the growth of the separation bubble is evident. The maximum reversed flow velocity captured in this dataset is about 10% of the bulk velocity and the separation bubble has grown to 75% of the inlet channel height. Figure 6 shows velocity vectors for the pulsed forcing case, which has the best pressure recovery of the three cases. The effects of the adverse pressure gradient are again clearly evident, but in this case, the actuators delay separation along the bottom wall. The separation bubble is smaller at the most downstream location and the peak reversed flow is only 5% of the bulk velocity. Delayed separation which yields a smaller separation bubble contributes to the improved pressure recovery for this case. The mean velocity profiles for the continuous forcing case in Figure 7 show very slow flow near the wall. Although slow, the mean velocity is still positive. The streamwise and vertical normal stresses reconcile the lack of reversed flow in the mean velocity profiles with the degraded pressure recovery for the continuous forcing case. Figures 8 and 9 show streamwise and vertical normal stresses for all three cases at one representative streamwise location, $x/h = 9.5$. While the values for both the streamwise and the vertical normal stresses are amplified for both of the plasma actuator cases, the values for the continuous forcing case are consistently larger. The largest streamwise normal and vertical normal stresses for this case are 30% and 50% higher than those in the baseline case. This suggests that the flow is highly unsteady with a separation bubble that fluctuates significantly. The separated flow is not captured in the mean velocity profiles as the unsteadiness and the movement of the separation bubble averages to slow positive streamwise velocities. The Reynolds shear stresses, not shown, are similar for all three cases.

In order to observe reversed flow in the mean for the continuous forcing case, data were acquired in the $50.4mm$ plane, closer to the expanding sidewall. The measurements

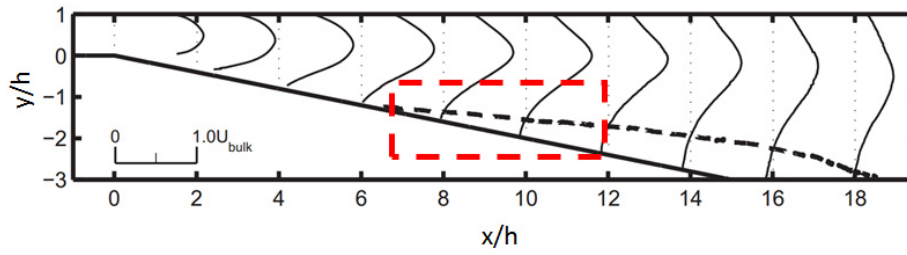


Figure 4. Side view of the diffuser showing profiles of streamwise velocity obtained by Kolade (2010) and a dotted rectangle outlining the measurement location for Figures 5 through 7.

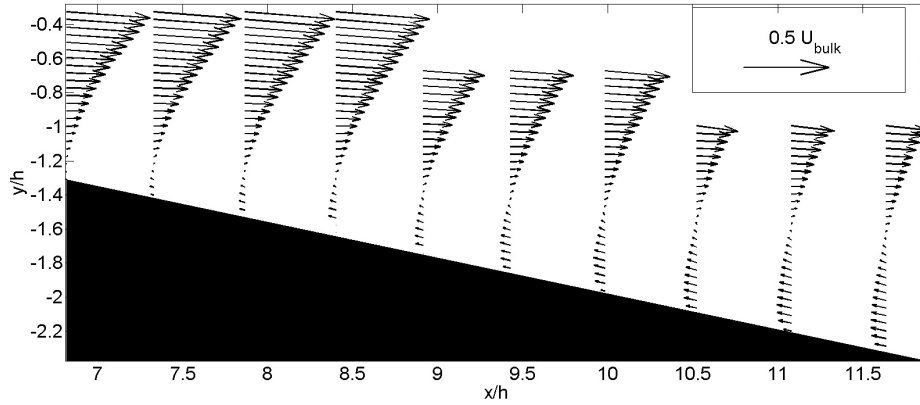


Figure 5. Mean velocity vector plot for the baseline case in the 25.4mm plane. The velocities are non-dimensionalized using the inlet bulk velocity of 10m/s.

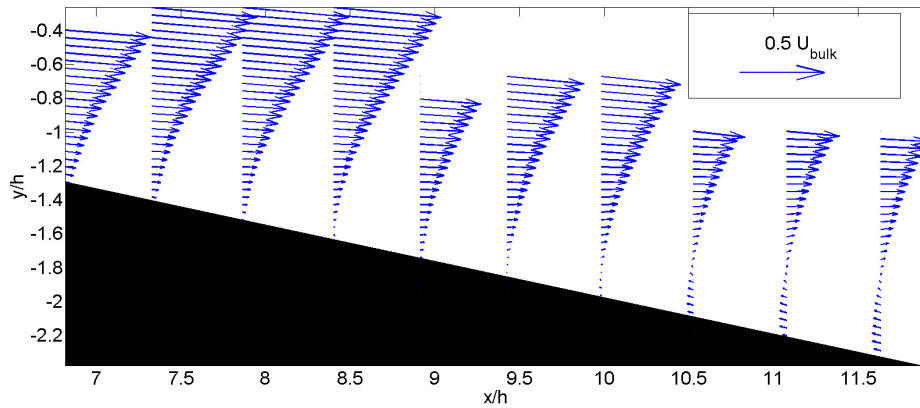


Figure 6. Mean velocity vector plot for the pulsed forcing case in the 25.4mm plane. The velocities are non-dimensionalized using the inlet bulk velocity of 10m/s.

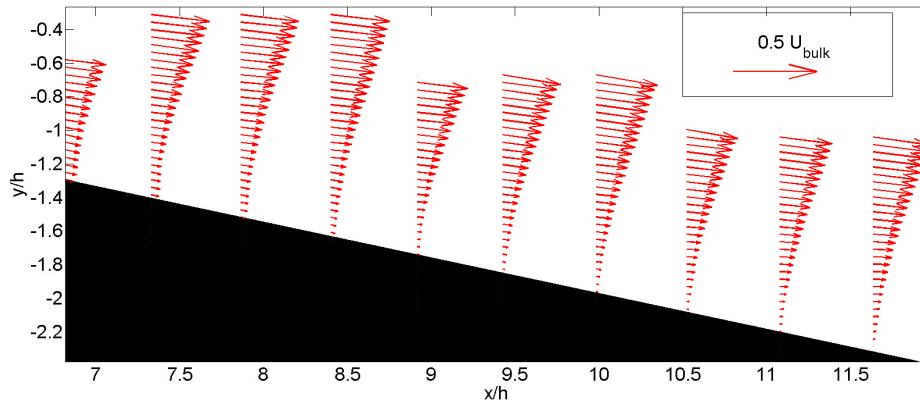


Figure 7. Mean velocity vector plot for the continuous forcing case in the 25.4mm plane. The velocities are non-dimensionalized using the inlet bulk velocity of 10m/s.

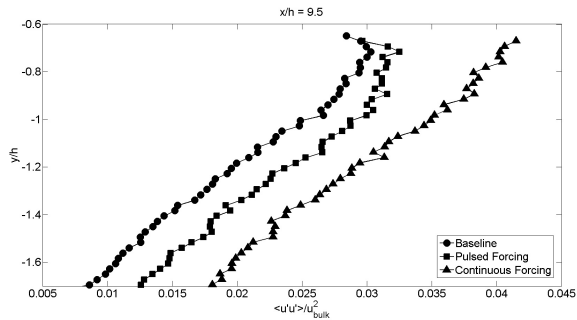


Figure 8. Streamwise normal stresses for all three cases at one streamwise location, ($x/h = 9.5$), in the 25.4mm plane.

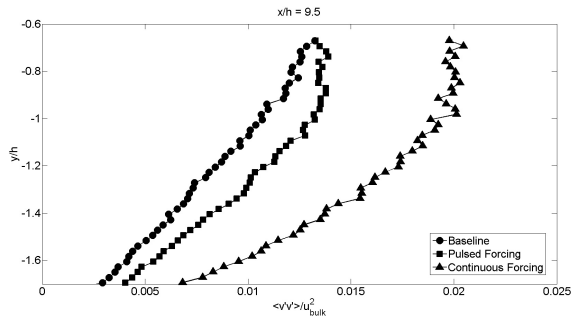


Figure 9. Vertical normal stresses for all three cases at one streamwise location, ($x/h = 9.5$), in the 25.4mm plane.

extend farther upstream since the separated flow region in the baseline case originates at the very beginning of the expansion along the edge shared by the expanding bottom and side walls. Figure 10 shows velocity vectors for the baseline case. As expected, the diffuser has stalled and the separation bubble grows moving downstream. The pulsed forcing case, shown in Figure 11, again yields a smaller separation bubble with lower reversed flow velocities when compared to the baseline case. In this plane, reversed flow does appear in the mean velocity profiles for the continuous forcing case, as seen in Figure 12. Compared to the other two cases, the separation bubble is significantly larger. Peak reversed flow velocities are nearly 20% of the bulk velocity, compared to 10% in the baseline case. Unlike the 25.4mm plane, the streamwise normal stresses are similar for all three cases. Only a slight increase in vertical normal stresses for the continuous forcing case was observed. Again, the Reynolds shear stresses for the three cases are similar in this measurement plane.

CONCLUSIONS

2D PIV was used to document the sensitivity of separated flow in a three-dimensional, asymmetric diffuser to dielectric barrier discharge plasma actuator-induced inlet condition perturbations. Secondary flows generated by spanwise-forcing actuators in the inlet channel were used to manipulate the flow's downstream separation behavior. PIV measurements revealed that these secondary flows significantly altered the pressure recovery of the diffuser by changing the shape and size of the separation bubble. The pulsed forcing case improved the diffuser's pressure recovery by delaying separation and thereby reducing overall losses. A smaller separated flow region with lower reversed flow velocities was observed in both measurement planes. Turbulent fluctuations in the continuous forcing case are evidence of significant unsteadiness and an unstable separation bubble. Measurements from a plane closer to the sidewall show a large separation bubble with very high reversed flow velocities which contribute to the early losses in pressure recovery observed for this case.

ACKNOWLEDGMENTS

This work was funded by the Office of Naval Research, Award Number N000141110319. Emily L. Sayles is supported by a Stanford Graduate Fellowship.

REFERENCES

- Cherry, E. M., Elkins, C. J. & Eaton, J. K. 2008 Geometric sensitivity of three-dimensional separated flows. *International Journal of Heat and Fluid Flow* **29** (3), 803–811.
- Grundmann, S., Sayles, E. L. & Eaton, J. K. 2011 Sensitivity of an asymmetric 3d diffuser to plasma-actuator induced inlet condition perturbations. *Experiments in Fluids* **50** (1), 217–231.
- Grundmann, S., Sayles, E. L., Elkins, C. J. & Eaton, J. K. 2012 Sensitivity of an asymmetric 3d diffuser to vortex-generator induced inlet condition perturbations. *Experiments in Fluids* **52** (1), 11–21.
- Han, D. 2001 Study of turbulent nonpremixed jet flames using simultaneous measurements of velocity and ch distribution. PhD thesis, Stanford University, Stanford, CA.
- Kolade, B. O. 2010 Experimental investigation of a three-dimensional separated diffuser. PhD thesis, Stanford University, Stanford, CA.
- Ohlsson, J., Schlatter, P., Fischer, P. F. & Henningson, D. S. 2010 Direct numerical simulation of separated flow in a three-dimensional diffuser. *Journal of Fluid Mechanics* **650**, 307–318.

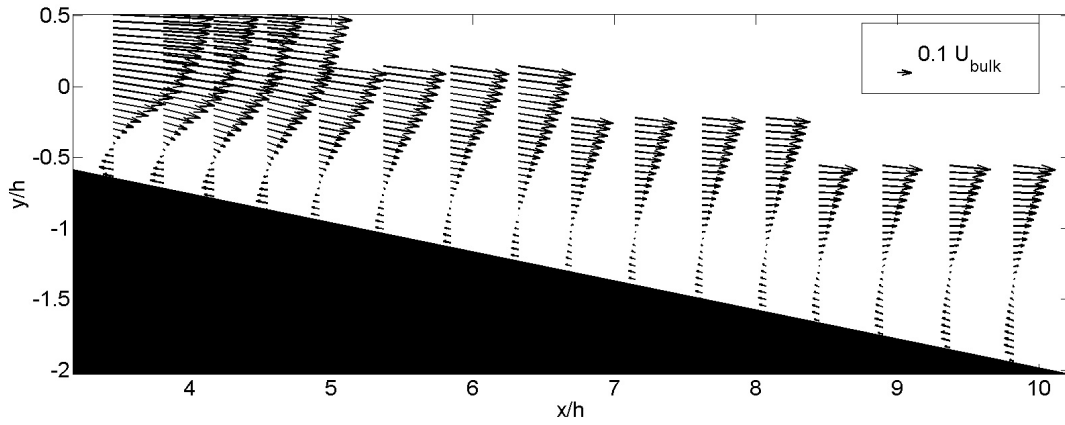


Figure 10. Mean velocity vector plot for the baseline case in the 50.8mm plane. The velocities are non-dimensionalized using the inlet bulk velocity of 10m/s.

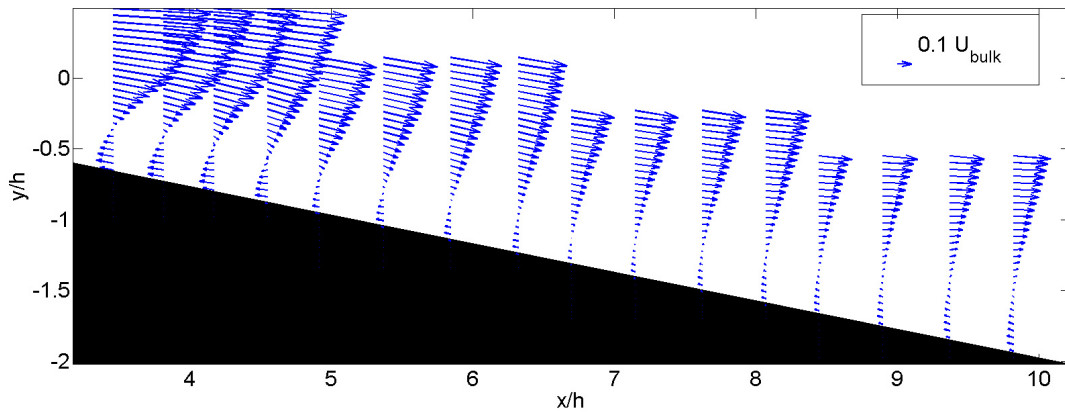


Figure 11. Mean velocity vector plot for the pulsed forcing case in the 50.8mm plane. The velocities are non-dimensionalized using the inlet bulk velocity of 10m/s.

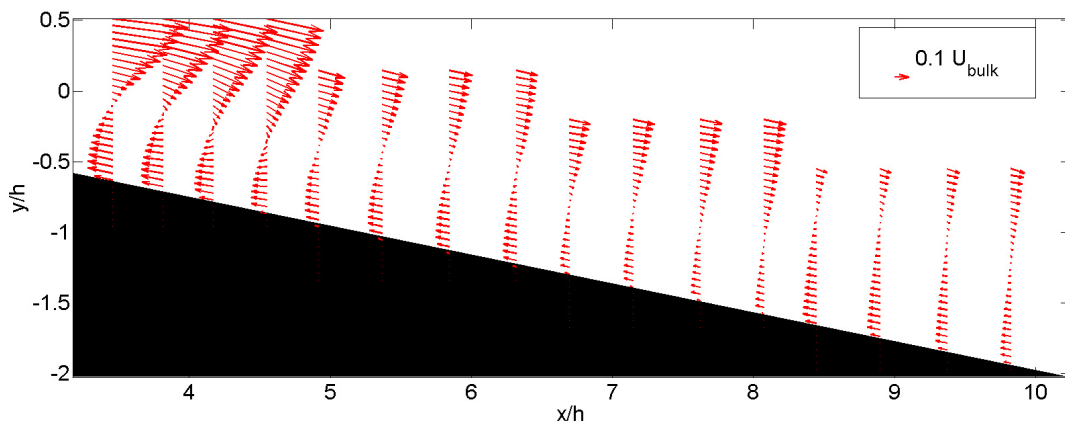


Figure 12. Mean velocity vector plot for the continuous forcing case in the 50.8mm plane. The velocities are non-dimensionalized using the inlet bulk velocity of 10m/s.